Measurements and Observations of Turbulent Recirculating Jet Flows

F. K. Owen*
United Technologies Research Center, East Hartford, Conn.

An extensive study has been made of the initial mixing regions of free and confined coaxial air jets with recirculation. Measurements of the axial and radial mean velocity profiles show that the time-averaged characteristics of the two flowfields are substantially different, and that significant mean radial velocities are present in both test cases. Root mean square (rms) and probability density distributions of the instantaneous velocity fluctuations define extensive regions of large scale motion associated with recirculation.

Introduction

TURBULENT shear flows with recirculation are an integral part of many engineering fluid mechanical configurations. These features may be deliberately introduced in the case of turbulent diffusion flame holders for instance, or they may be unintentional features resulting in a significant decrease in performance, stalled aerofoils being a good example. At the present time, determined efforts are being made using combined experimental and computational techniques to increase our understanding and ability to predict these complex shear flows. To date, these efforts have met with only restricted success due to limitations in both approaches.

Although significant progress has recently been made in the field of computational fluid dynamics due mainly to improved numerical techniques and increased computing capacity, the calculation of turbulent flows is still only a practical proposition when the turbulent corrections ($\overline{u'v'}$ for example) which arise from the process of time-averaging the Navier-Stokes equations can be modeled by simple mixing length or turbulent kinetic energy assumptions. It is difficult to assess the ability of present calculation procedures to predict complex turbulent flows of practical interest for two reasons; namely, the lack of adequate time averaged flowfield measurements which could provide reliable test cases, and the lack of turbulent structure information which could be used to assess the validity of present models or illustrate their shortcomings and guide the formulation of improved models to account for turbulent nonequilibrium effects.

Recirculating flows pose problems to experimentalists since flowfields with severe adverse pressure gradients which normally give rise to separation, and recirculation are difficult to document as they are extremely sensitive to local geometry and probe interference. In addition, streamline curvature and associated static pressure variations make conventional mean flow instrumentation techniques unreliable. Problems associated with turbulence structure measurements are even more acute because linearized hot wire data interpretations are not accurate in these highly turbulent flows. Fortunately, with the advent of the laser velocimeter, fluid mechanical measurements are now possible without perturbing the flowfield. This is true provided light scattering particles can be relied upon to follow the local fluid velocity. This technique with its inherent linear sensitivity enables quantitative documentation of recirculating flows.

Accordingly, a comprehensive laser velocimeter study has been made of two flowfields with recirculation. The aim of the work is to provide reliable measurements of complex turbulent flows which can be used as test cases to assess present calculation procedures and to provide additional insight into the turbulent structure of recirculating flows.

Received Feb. 23, 1976; revision received May 17, 1976.
Index category: Jets, Wakes and Viscid-Inviscid Flow Interactions.
*Senior Research Engineer. Member AIAA.

Experimental Details

The measurements were made in the initial mixing region of two coaxial air jets which are shown schematically in Fig. 1. Two geometrical configurations were studied; namely, a free expansion into the laboratory and a confined expansion into a 5.0 in. diameter, 48.0 in. long tube. In each case the outer and inner peak velocities were 96.0 and 8.0 fps corresponding to Reynolds numbers based on respective jet diameters of 1.5 and 0.08×10^5. In both cases the outer to inner jet velocity ratio was sufficient to produce a recirculation zone in the initial mixing region above the center jet. In the confined case an additional recirculation zone occurred in the corner between the outer jet and the confining duct.

The mean velocity and turbulence measurements were made using a dual beam velocimeter with which zero velocity frequency offset was achieved using a Bragg cell.[1] This enabled the sign as well as the magnitude of the instantaneous velocities to be determined as follows

$$U=\frac{(f_D-f_0)\lambda}{2\sin\theta/2} \tag{1}$$

where f_D and f_0 are the moving and stationary particle doppler frequencies, λ is the wavelength of the laser light, and θ is the angle between the two incident laser beams. This system of interference fringes moving across the focal volume precluded the possibility of data interpretation errors which can occur in highly turbulent and/or recirculating flows.[1]

Single particle, time domain signal processing was used to build up the velocity probability density distributions from which both mean velocities and rms velocity fluctuations were obtained using the following equations

$$\bar{U}=\sum_{i=1}^{N}\frac{U_i}{N} \tag{2}$$

$$\sigma=\sqrt{\overline{u'^2}}=\left(\sum_{i=1}^{N}\frac{U_i^2}{N}-\bar{U}^2\right)^{1/2} \tag{3}$$

In the present experiments, a minimum of 2000 instantaneous velocity determinations was used to build up the probability densities which resulted in a statistical error of less than 5% in the computed values of both the mean and variance with a confidence level of 95%. Indeed, for the confined flow, where a mass balance could be made, the mass flow computed from the measured mean velocity profile agreed to better than 5% with the metered air supply.

Various degrees of sensitivity to the instantaneous axial and radial velocities can be achieved by rotating the Bragg cell about an axis coincident with the laser beam. With the beams in the axial plane $\bar{U}$ and $\overline{u'^2}$ are determined from Eqs. (2) and (3). With the beams orientated at $\pm 45°$ to the axial plane, $\bar{V}$, $\overline{u'v'}$, and $\overline{u'^2}+\overline{v'^2}$ can be determined by vector addition of Eq. (2) and the difference and sum of the variances (Eq. (3)), respectively. Assuming $\overline{w'^2}=0(\overline{u'^2})=0(\overline{v'^2})$ the sum of the variances is proportional to the local turbulent kinetic energy q^2. This will be implicit during the discussion of the turbulence measurements in the paper.

The optical sensitivity of the present forward scatter system was such that naturally occurring submicron particles were used for the velocity determinations. For these flows more than 95% of the turbulence energy is in scales corresponding to Eulerian frequencies below 20 KHz so that errors due to particle response (in the Lagrangian frame) are negligible. The sensing volume determined by beam crossover, off axis collection, and photo-multiplier pin hole size resulted in elliptic spatial resolution with principle axes of 0.010 in. and 0.080 in., respectively.

In the confined flow region downstream of the annular backward facing step fluctuation measurements were made using thin platinum films deposited on pyrex glass substrates which were mounted flush with the inside tube surface. Gage construction and constant temperature operation was identical to that described in Ref. 2. Visualization of wall-jet impingement locations were identified from the build up of airborne particle deposits which was achieved by seeding the air flow with geon particles dispensed from a fluidized bed.

Results

Mean Flow Measurements

Centerline mean axial velocity and turbulent intensity profiles for the free expansion are shown in Fig. 2. The mean flow measurements show that there is a region of "time averaged" reverse flow extending from a point near the nozzle exit to approximately 2.75 in. from the exit plane. The peak reverse flow velocities are a significant fraction (close to 50%) of the maximum centerline streamwise velocity. Axial velocity profiles measured between 1.0 and 4.0 in. from the nozzle exits are shown in Fig. 3. These data show the lateral extent of the recirculation zone and a consistent trend towards a self similar profile which would be expected well downstream of the initial mixing region.

With the aid of the continuity equation, stream functions can be obtained by integrating the radial distributions of mean axial velocity shown in Fig. 3. From the radial distribution of these system functions

$$\psi=\int_0^r \rho\bar{U}dr$$

at a number of axial stations, streamlines can be drawn through points of constant ψ. These values nondimensionalized by

$$\psi_0=\int_0^{d_0/2} \rho\bar{U}rdr$$

(determined from the nozzle exit velocity profiles) are shown in Fig. 4. This streamline distribution shows the time-averaged fluid dynamic characteristics of the recirculation zone; namely, its size and the recirculated mass flow compared to the nozzle geometry and total mass flow, respectively. Inward movement of the dividing streamline between the inner and outer jet downstream of the recirculation zone indicates entrainment of the inner jet by the faster moving outer flow. Entrainment of ambient fluid can also be inferred from the values of $\psi/\psi_0 > 1.0$ in the outer flowfield.

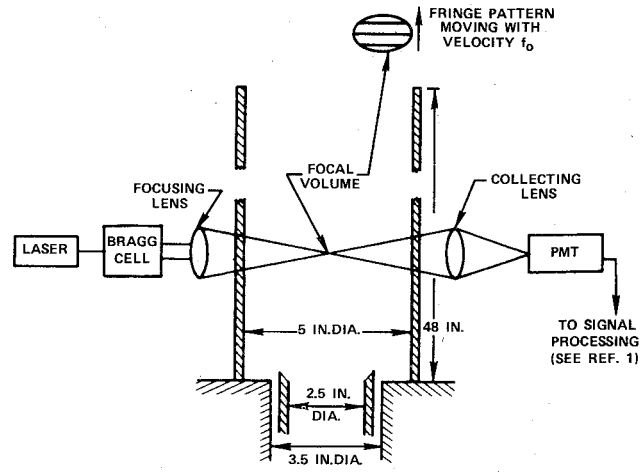

Fig. 1 Schematic of the laser velocimeter and the confined flow geometry.

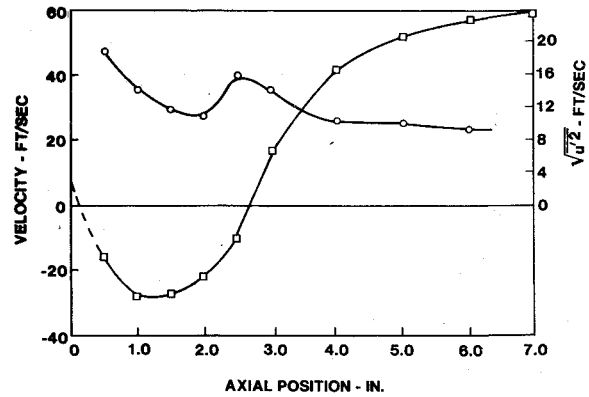

Fig. 2 Axial velocity measurements along centerline for the free expansion, □ – Mean velocity, ○ – rms velocity fluctuation.

Mean radial velocities obtained by vector addition of the mean velocities normal to the fringes with Bragg cell orientations of $\pm 45°$ to the axial plane are presented in Fig. 5. These results are in general agreement with the streamlines constructed from the axial velocity profiles showing flow around the bubble and entrainment by the outer jet. The data also show that the mean radial velocities and their gradients are significant fractions of the corresponding axial velocity values which is of importance for momentum field and turbulent shear stress formulations.

The confined centerline mean axial velocity and turbulent intensity profiles are presented in Fig. 6. Comparison with equivalent data for the free expansion shows that, although the turbulent fluctuation levels are similar, the longitudinal extent of the recirculation zone is significantly larger in the confined flow, and that the corresponding mean reverse velocities are a larger percentage of the maximum centerline axial velocity. The axial velocity profiles presented in Fig. 7 also show that the lateral extent of the confined recirculation zone is much larger than in the free expansion. The velocity profile at the $x=1.25$ in. station also shows evidence of a second recirculation zone behind the backward facing step at the nozzle exit plane. This is an important mechanism in the confined flow and will be discussed in detail later in the paper.

Again these axial velocity profiles were integrated and mean streamlines obtained as described previously. A comparison of these results presented in Fig. 8a and those for the free expansion (Fig. 4) confirms that there are significant increases in both the longitudinal and lateral extent of the recirculation zone for the confined case. As shown in Fig. 8b, this large recirculation zone has a pronounced effect on the mean flow field; namely, flow curvature around the bubble resulting in a

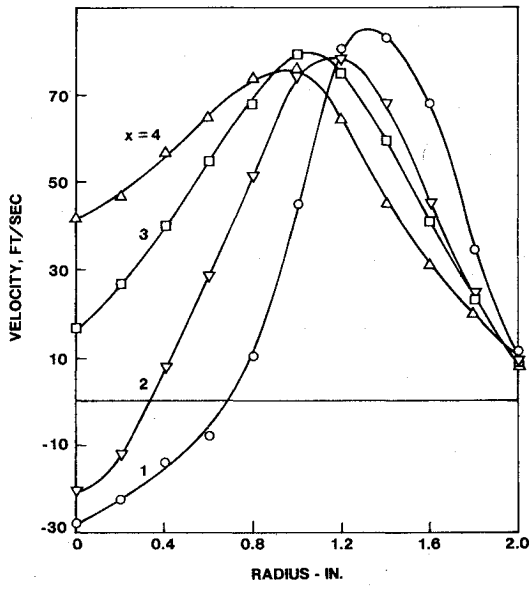

Fig. 3 Mean axial velocity profiles for the free expansion.

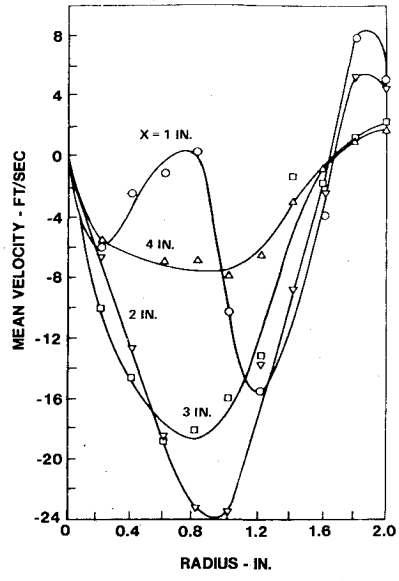

Fig. 5 Mean radial velocity profiles for the free expansion.

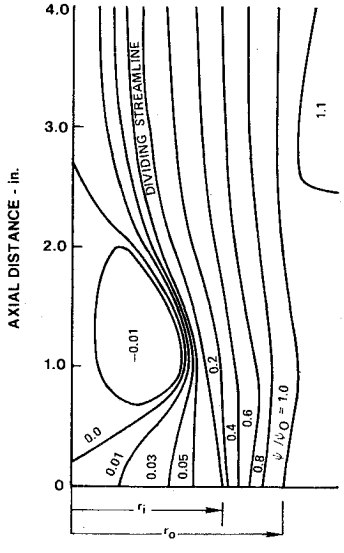

Fig. 4 Streamline distributions for the free expansion.

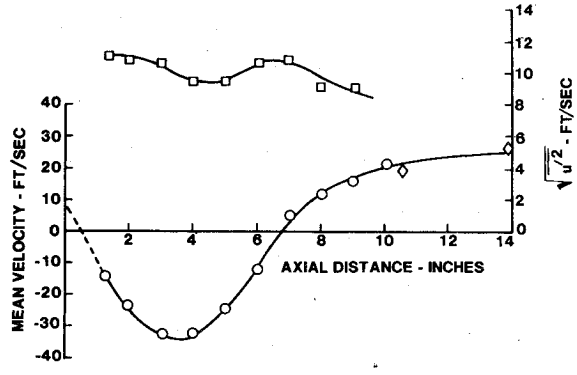

Fig. 6 Axial velocity measurements along the nozzle centerline for the confined expansion, □ – Mean velocity, ○ – rms velocity fluctuation, ◇ – Pitot tube.

high shear layer in the outer annulus close to the wall. Mean raidal velocity measurements have also been made (Fig. 9) and are in good agreement with the streamline and axial velocity contours of Fig. 8; i.e., mean flow outwards around the bubble at $x = 1.25$ in. and mean flow inwards behind the bubble at the $x = 5.0$ and 9.0 in. stations.

These mean flowfield measurements in the initial mixing regions of free and confined coannular air jets show that there are large differences in the time-averaged structure of the two flowfields. One significant difference between the two flows is the variation of reverse mass flow (W) within the two recirculation zones shown in Fig. 10. This figure emphasizes the fact that the size and recirculation mass flux are significantly larger in the confined flow than in the free expansion. In the confined flow, the bubble has a length and maximum lateral extent of approximately 1.0 and 0.5 confining duct diameters, respectively, and a maximum reverse mass flow rate of nearly an order of magnitude larger than in the free expansion. This is almost twice the inner jet mass flow and 20% of the total jet efflux. The reason for this difference between the two flows is thought to be due to the more rapid expansion of the outer jet in the confined case which is caused by the lack of available entrainment air. This results in jet attachment close to the nozzle exit and a sharp increase in static pressure which is encountered by the inner jet. Thus, for fixed inner jet momentum, recirculation is more pronounced in the confined flow.

Turbulence Measurements

Measurements of the axial turbulent intensities along the flowfield centerline for the free and confined flows are shown in Figs. 2 and 6. These data show that in both cases the turbulent fluctuation levels are extremely high in the initial mixing regions and have local maxima close to the time-averaged axial velocity zeros. These peaks at either end of the time averaged recirculation zone are an indication of large scale recirculation zone movement about its mean location. This will be discussed later.

Free expansion measurements of the local axial and radial rms velocity fluctuations are compared with the axial mean velocity profile in Fig. 11. These measurements made 3 in. from the nozzle exit plane show that the local turbulence levels vary with the magnitude of the mean velocity gradient. This variation of turbulence level with mean velocity profile occurs throughout the initial region.[1] However, calculations show that a simple (constant) mixing length relationship cannot be applied to predict either the axial or radial velocity fluctuations.

Data taken at the $x = 2.0$ in. location shown in Fig. 12 compare two components of the local turbulent kinetic energy ($q^2 = \overline{u'^2} + \overline{v'^2}$) and the turbulent shear stress distribution ($\overline{u'v'}$). Although the two curves are qualitatively similar at this location and throughout the initial mixing region,[1] simple

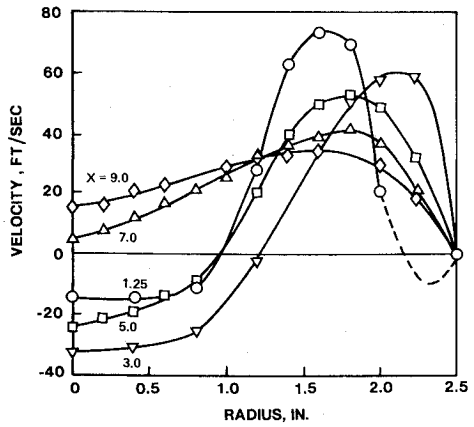

Fig. 7 Mean axial velocity profiles for the confined expansion.

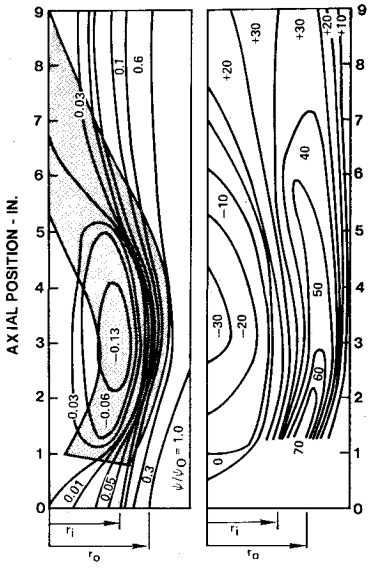

Fig. 8 Mean streamline and axial velocity contours for the confined expansion.

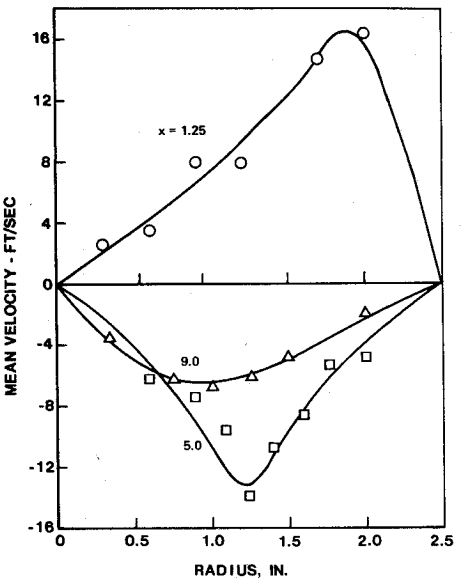

Fig. 9 Mean radial velocity profiles for the confined expansion.

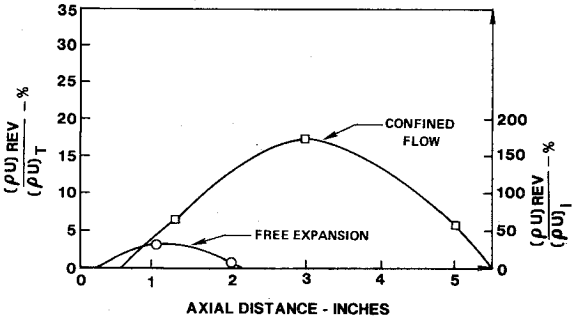

Fig. 10 Comparison of the mass flow recirculation rate distributions for the free and confined flowfields.

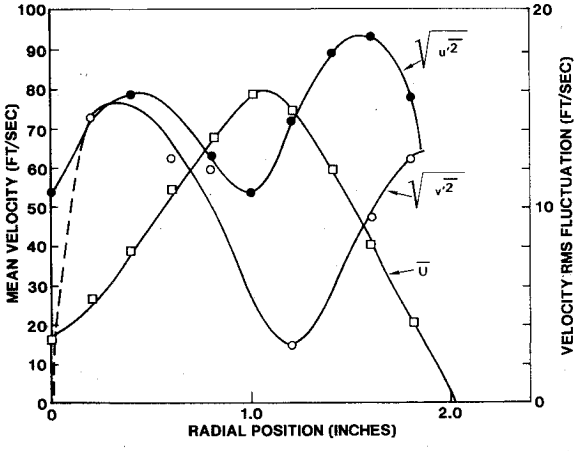

Fig. 11 Mean velocity and rms turbulent velocity profiles three inches from the nozzle exits for the free expansion.

proportionality relationships between the two variables, which work well in boundary-layer type flows for which they were devised, cannot be used since the shear stress changes sign. This sign change is accounted for in both the mixing length hypothesis, i.e.,

$$\overline{u'v'} = \ell^2 \frac{d\bar{U}}{dy}\left|\frac{d\bar{U}}{dy}\right|$$

and the Kolmogorov relationship $\overline{u'v'} = q\ell(d\bar{U}/dy)$, but mixing length constants which are usually used in these formulations for free shear layer computations are inadequate to predict the shear stress distribution in this flowfield. Similar drawbacks in the confined expansion case are also apparent.[1]

In addition, the mean radial velocities measured in the initial mixing regions of both flowfields are the same order of magnitude as the mean axial velocities. Therefore, the usual boundary-layer type approximations cannot be made in these regions, and the full Navier-Stokes equations may have to be used in the analysis of these flowfields.

Unsteady (Large Scale Turbulent) Aspects of Recirculating Flows

Consider first the sequence of events during the establishment of the confined jet flow: initially the flow will behave like a free expansion until the jet attaches to the tube wall well downstream of the initial mixing region. However, unlike the free expansion, there is a limited supply of "stagnant" air to provide free shear layer entrainment so that a drop in pressure must occur behind the rearward facing step which results in upstream movement of the time-averaged attachment point to a position closer to the nozzle exit plane.

The unsteady aspects of this attachment point movement first became apparent during flow symmetry studies in which the air flow was seeded with geon particles to determine wall impingement locations. This test resulted in a ring of geon deposit on the tube wall extending from approximately 2.0 to 3.5 in. from the nozzle exits. It was felt that this range of particle deposits was an indication of the extent of the instantaneous attachment point movement.[3] This interpretation

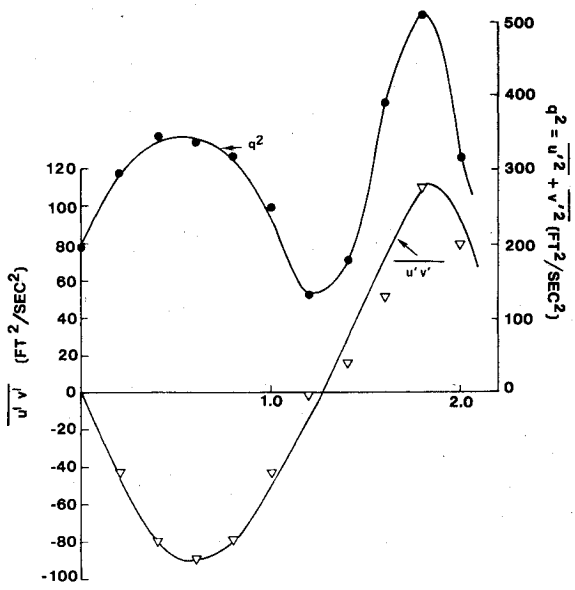

Fig. 12 Turbulent shear stress and kinetic energy profiles two inches from the nozzle exits for the free expansion.

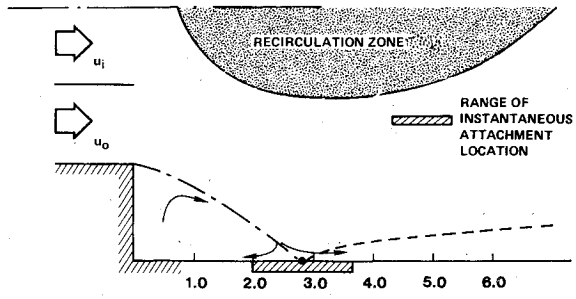

Fig. 13 Outer jet attachment flow model.

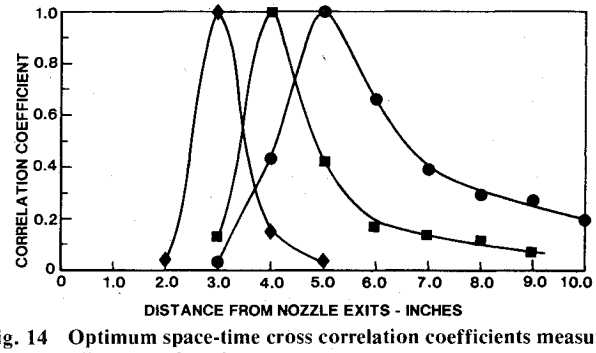

Fig. 14 Optimum space-time cross correlation coefficients measured relative to fixed gage locations.

is supported by the subsequent surface hot film turbulent cross correlation measurements. The flow behind the rearward facing step deduced from these surface thin film gage cross correlations is shown schematically in Fig. 13.

In this model the shear layer is assumed to split at the instantaneous attachment point; the upstream flow providing fluid for the free shear layer entrainment from the corner recirculation zone. Thus, one would expect little if any correlation between the turbulent fluctuations on either side of the instantaneous attachment range, i.e., between the 2.0 and 4.0 in. locations, improved correlation between the 2.0 and 3.0 and the 3.0 and 4.0 in. stations since both will sense the same disturbances during the times that the attachment point is downstream and upstream of the 3.0 in. location, respectively, and good correlation between the turbulent fluctuations at stations downstream of the attachment region.

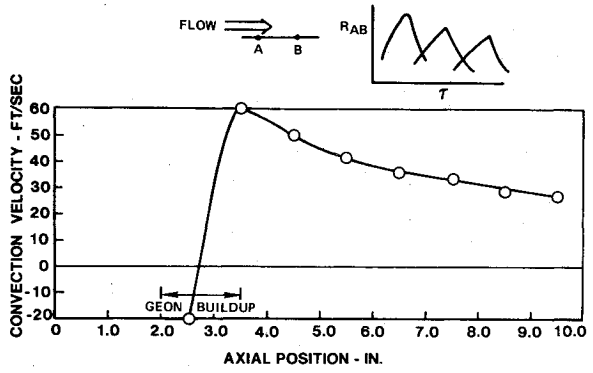

Fig. 15 Turbulence convection velocities obtained from space-time cross correlation measurements.

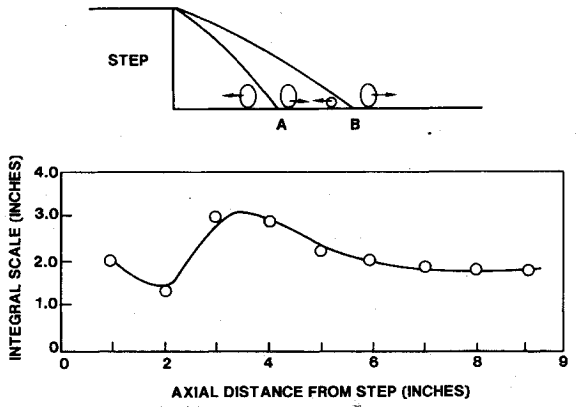

Fig. 16 Model and measurements of the integral scales of turbulence in the wall region.

These are the trends which are observed in the optimum space time correlation measurements presented in Fig. 14. Turbulence convection velocity measurements determined from the known gage separation and the time delay (τ) for optimum cross correlation also confirm the model since they show a time-averaged reverse flow velocity in the corner region, and high forward velocity ($\bar{U}_c/\bar{U}_\infty = 0.8$) in the thin wall shear layer immediately downstream of the attachment region (see Fig. 15).

Two possible causes and related observations for such extensive movement of the instantaneous attachment point around its time-averaged position will now be discussed. Since the mean attachment location reflects the balance between time-averaged entrainment and upstream deflection rates so the instantaneous attachment point movement reflects the imbalance between the local instantaneous entrainment and upstream deflection rates. Since the instantaneous entrainment rate is related to the turbulence scales in the free shear layer,[4] one would expect random movements of the instantaneous attachment point due to local imbalances between entrainment from, and supply to, the recirculation zone. This entrainment mechanism would not give rise to either axial or spanwise periodic fluctuations in the attachment region, which was the case. This mechanism would also result in random distortion of the instantaneous attachment point around the tube which should be related to the lateral turbulence scale (Λ_{zz}). Thus, lateral space-time correlations in the attachment region should be small compared to equivalent longitudinal measurements since $\Lambda_{zz} >> \Lambda_{xx}$. Lateral space-time correlation measurements have confirmed this observation, since they were indeed small compared to the axial measurements shown in Fig. 14.

Turning now to the splitting of the shear layer at attachment we can consider a second mechanism for attachment point movement. Bradshaw and Wong[5] supposed that the

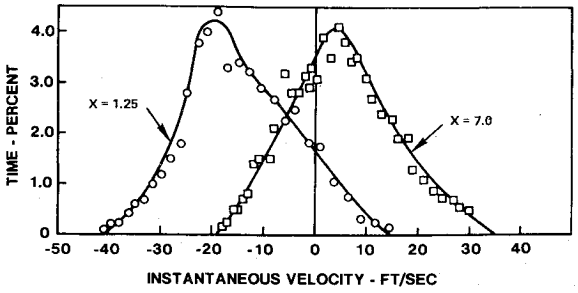

Fig. 17 Axial velocity probability density distributions obtained on the centerline for the confined expansion.

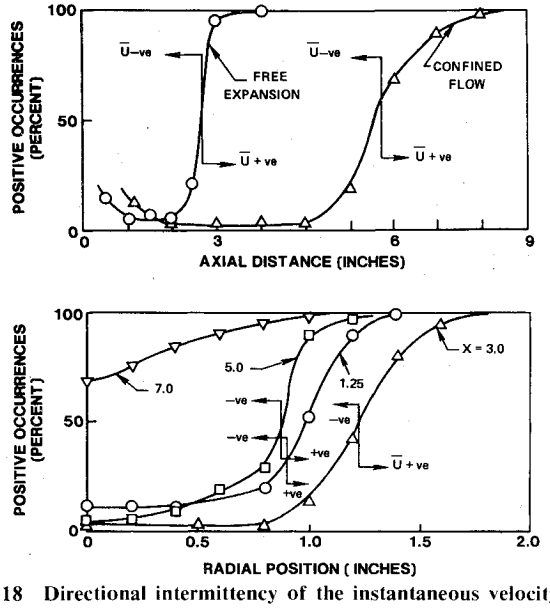

Fig. 18 Directional intermittency of the instantaneous velocity occurrences.

fraction of the shear layer mass flow deflected upstream would depend on the initial boundary-layer thickness. Since this simple model must breakdown at the asymptotic limit of zero initial boundary-layer thickness, it is intuitively expected that the recirculated mass flow would also depend on the angle of attachment. At attachment (see Fig. 16), one would expect most eddy tearing resulting in smallest wall turbulent length scale, when the instantaneous attachment point is close to the nozzle exits. This decrease in turbulence length scale in the attachment region is confirmed by the integral length scale data in Fig. 16. This eddy tearing variation shown schematically in Fig. 16 is an additional source of attachment point fluctuations. Since when the free shear layer attaches at point A, least fluid is entrained from and most fluid deflected into the corner recirculation zone; thus, eventually the upstream static pressure within the recirculation zone will increase resulting in attachment point movement downstream. Conversely, at the downstream limit of attachment (Point B) maximum entrainment and minimum upstream deflection occur resulting in a pressure drop in the recirculation zone with subsequent upstream attachment movement.

Quantitative insight into the large scale turbulent (unsteady) nature of the central recirculation zone, may be obtained from the velocity probability density distributions such as those shown in Fig. 17. These measurements, which can only be obtained with zero velocity frequency offset, show the unsteadiness of the flowfield in the initial mixing region. For the confined expansion, within the time-averaged recirculation zone ($x=1.25$ in.), there are significant numbers of positive velocity occurrences (approximately 12%) which may be the result of bubble breakdown and/or movement up and downstream. Conversely, just beyond the recirculation zone ($x=7.0$ in.), instantaneous negative velocities are present approximately 30% of the time, possibly the result of instantaneous bubble expansion and/or movement downstream. Such velocity probability measurements enable directional intermittency of the instantaneous axial velocities to be determined. Examples of measurements obtained on the centerline of the free and confined flow and at radial stations downstream of the nozzle exit plane in the confined flow are shown in Figs. 18a and b. These directional intermittency data provide valuable insight into the structure of the flow in the region of the recirculation zone. Namely, well within the time-averaged recirculation zone there are significant numbers of positive velocity occurrences (15%) which suggest periods of large scale bubble movement downstream. Conversely, the probability of such large reverse velocities just inside the boundary of time-averaged zones, which are evident in Fig. 17, suggest periods of extensive bubble movement upstream. Such unsteadiness would also produce peaks in turbulence intensity at either end of the time-averaged recirculation zone as noted previously and shown in Figs. 2 and 6. These peaks can be explained qualitatively by considering the various sources of the total velocity fluctuations (u_T'); namely, the turbulent fluctuations associated with forward and reverse flow (u' and u_{Rev}', respectively) and the additional source due to sign change of mean velocity ($\bar{U}-\bar{U}_{\mathrm{Rev}}$) at the point in question. So we may write

$$u_T'(x)=f\{\gamma_x u', (1-\gamma)u_{\mathrm{Rev}}', n(x)_x(\bar{U}-\bar{U}_{\mathrm{Rev}})\} \quad (4)$$

where γ_X is the percentage of time the mean flow is downstream and n_X is the frequency of mean flow reversal. Now defining

$$n(x)=A+B(d\gamma/dx) \quad (5)$$

which satisfies the intuitive expectation that the frequency of mean flow reversal should have maxima near the edges of the time-averaged recirculation zone and, since $\bar{U}-\bar{U}_{\mathrm{Rev}}=0(u')=0(u_{\mathrm{Rev}}')$, inspection of Fig. 18 suggests that the downstream maximum centerline local total velocity fluctuations should occur at approximate axial locations of 2.5 and 6.5 in. for the free and confined flows, respectively. This is confirmed in Figs. 2 and 6.

By analogy to the range of instantaneous attachment behind the rearward facing step (Fig. 13), an equivalent range of instantaneous rearward stagnation point axial locations can be determined from Fig. 18a for both central recirculation zones. In the free expansion, the range of instantaneous downstream stagnation points extends from approximately 2.0 to 3.0 in. from the nozzle exit plane with a time-averaged location of approximately 2.7 in. In the confined case, the range is approximately 5.0 to 9.0 in. about a mean location of 6.7 in. Lateral ranges of unsteadiness can also be determined in a similar manner from Fig. 18b. This range of large scale fluctuations (the shaded area) is shown compared with the location of the confined time-averaged recirculation zone in Fig. 8. It is felt that the reasons for this longitudinal and lateral large scale unsteadiness are similar to those discussed previously for the corner recirculation zone; namely, time dependent entrainment from the stagnation points upstream deflection into, the central recirculation zone.

Concluding Remarks

The usefulness of a frequency-offset laser velocimeter for both mean and turbulence measurements in recirculating flows has been demonstrated. Measurements in the initial mixing regions of free and confined coannular air jets have shown that there are large differences in the time-averaged structure of the two flowfields, the size and recirculation mass flux being significantly larger in the confined flow than in the free expansion.

The mean radial velocities measured in both initial mixing regions are the same order of magnitude as the mean axial velocities. Therefore, the usual boundary-layer approximations cannot be made in this region, and the full time-averaged elliptical equations may have to be used in the analysis of these flowfields. The measured turbulent intensities and shear stress distributions in recirculation regions show that local turbulence equilibrium models are inadequate. These data indicate that higher order turbulence models which account for local structural nonequilibrium will probably be required to compute these flows.

Velocity probability density distributions and associated directional intermittency measurements indicate that there is a substantial large-scale contribution to the total rms turbulent velocity flowfield. Such large-scale motions also indicate that turbulence models based on local equilibrium principles, such as mixing lengths and others which utilize local mean gradients, will not adequately represent the physics of these recirculating flows.

References

[1]Owen, F. K., "Laser Velocimeter Measurements in Free and Confined Coaxial Jets with Recirculation," AIAA Paper 75-120, Pasadena, Calif., 1975.

[2]Owen, F. K., "Transition Experiments on a Flat Plat at Subsonic and Supersonic Speeds," *AIAA Journal*, Vol. 8, March 1970, pp. 518-523.

[3]Abbott, D. E. and Kline, S. J., "Experimental Investigation of Subsonic Turbulent Flow Over Single and Double Backward Facing Steps," *Journal of Basic Engineering*, Vol. 84, Sept. 1962, pp. 317-325.

[4]Brown, G. L. and Roshko, A., "On Density Effects and Large Structure in Turbulent Mixing Layers," *Journal of Fluid Mechanics*, Vol. 64, July 1974, pp. 775-816.

[5]Bradshaw, P. and Wong, F.Y.F., "The Reattachment and Relaxation of a Turbulent Shear Layer," *Journal of Fluid Mechanics*, Vol. 52, March 1972, pp. 113-135.